



Disruption of *FLNB* leads to skeletal malformation by interfering with skeletal segmentation through the *HOX* gene

Qiming Xu^{a,*}, Lijia Cui^{b,1}, Yude Lin^c, Leigh-Anne Cui^d, Weibo Xia^{b,**}

^a Department of Orthopedic Oncology, Beijing Jishuitan Hospital, Capital Medical University, Beijing 100085, China

^b Department of Endocrinology, Peking Union Medical College Hospital, Chinese Academy of Medical Sciences and Peking Union Medical College, Beijing 100730, China

^c Bio-X Institutes, Key Laboratory for the Genetics of Developmental and Neuropsychiatric Disorders, Shanghai Jiao Tong University, Shanghai 200240, China

^d Department of Molecular Medicine, The Scripps Research Institute, La Jolla, CA 92037, USA

ARTICLE INFO

Keywords:

Filamin B

HOX

Skeletal segmentation

CRISPR-Cas9

In situ hybridization of embryo

ABSTRACT

Filamin B (FLNB) plays an important role in skeletal development. Mutations in *FLNB* can lead to skeletal malformation such as an abnormal number of ossification centers, indicating that the skeletal segmentation in the embryonic period may be interfered with. We established a mouse model with the pathogenic point mutation *FLNB* NM_001081427.1: c.4756G > A (p.Gly1586Arg) using CRISPR-Cas9 technology. Micro-CT, HE staining and whole skeletal preparation were performed to examine the skeletal malformation. *In situ* hybridization of embryos was performed to examine the transcription of *HOX* genes during embryonic development. The expression of *FLNB* was downregulated in *FLNB*^{G1586R/G1586R} and *FLNB*^{WT/G1586R} mice, compared to *FLNB*^{WT/WT} mice. Fusions in tarsal bones were found in *FLNB*^{G1586R/G1586R} and *FLNB*^{WT/G1586R} mice, indicating that the skeletal segmentation was interfered with. In the embryo of *FLNB*^{G1586R/G1586R} mice (E12.5), the transcription levels of *HOXD10* and *HOXB2* were downregulated in the carpal region and cervical spine region, respectively. This study indicated that the loss-of-function mutation G1586R in *FLNB* may lead to abnormal skeletal segmentation, and the mechanism was possibly associated with the downregulation of *HOX* gene transcription during the embryonic period.

1. Introduction

Filamin B is a cytoplasmic protein encoded by *FLNB*. Filamin B crosslinks with the actin cytoskeleton, provides a scaffold for many other molecules in the cell, and participates in signaling transduction (Stossel et al., 2001). Mutations in *FLNB* are associated with a spectrum of distinct skeletal dysplasia, indicating the important role of *FLNB* in skeletal development (Xu et al., 2017). Gain-of-function mutation in *FLNB* leads to Larsen syndrome, atelosteogenesis type I, atelosteogenesis type III, and boomerang dysplasia (Maroteaux et al., 1982; Jeon et al., 2014; Kozłowski et al., 1981; Tenconi et al., 1983; Kozłowski et al., 1985). These diseases present short stature and skeletal malformations including supernumerary ossification centers of carpal and tarsal bones,

and scoliosis (Larsen et al., 1950; Stanley et al., 1988). Loss-of-function mutation in *FLNB* leads to spondylorcarpotarsal synostosis syndrome (SCT syndrome), presenting skeletal malformations including premature fusions in carpal and tarsal bones, and fusions in vertebrae (Krakow et al., 2004).

These clinical manifestations above indicated that gain/loss-of-function mutations in *FLNB* might lead to changes in ossification centers, indicating that the skeletal segmentation might be interfered with during embryo development. However, previous researchers only reported that loss-of-function in *FLNB* inhibited the growth of long bone, which could explain the short stature of such patients (Hu et al., 2014; Lu et al., 2007; Daniel et al., 2012; Sawyer et al., 2009; Zheng et al., 2007). The mechanism of *FLNB* mutations interfering with the skeletal

* Corresponding author at: Department of Orthopedic Oncology, Beijing Jishuitan Hospital, Capital Medical University, No. 38 Longyuhuan Road, Changping District, Beijing 100085, China.

** Corresponding author at: Department of Endocrinology, Peking Union Medical College Hospital, Chinese Academy of Medical Sciences and Peking Union Medical College, No. 1 Shuaifuyuan, Dongcheng District, Beijing 100730, China.

E-mail addresses: xuqiming@jst-hosp.com.cn (Q. Xu), cuilijia@pumch.cn (L. Cui), linyudesjtu@sju.edu.cn (Y. Lin), lcui@scripps.edu (L.-A. Cui), xiawb@pumch.cn (W. Xia).

¹ Qiming Xu and Lijia Cui contributed equally as first authors.

<https://doi.org/10.1016/j.bonr.2024.101746>

Received 16 August 2023; Received in revised form 22 February 2024; Accepted 25 February 2024

Available online 28 February 2024

2352-1872/© 2024 Published by Elsevier Inc. This is an open access article under the CC BY-NC-ND license (<http://creativecommons.org/licenses/by-nc-nd/4.0/>).

segmentation process remains unclear.

Skeletal segment identity of vertebral animals is known to be specified by *HOX* genes in the embryo period (Quinonez and Innis, 2014). Over ten *HOX* genes have been reported to be associated with skeletal malformation. Interestingly, the skeletal malformation phenotypes were remarkably similar between the *HOX*-mutated spectrum disorders and *FLNB*-mutated spectrum disorders, both of which were characterized by alterations in the number of ossification centers (Xu et al., 2017; Quinonez and Innis, 2014).

In this study, we hypothesized that the loss-of-function mutation in *FLNB* led to skeletal malformation by interfering with skeletal segmentation through the *HOX* gene during the embryonic period. We established a mouse model with *FLNB* G1586R loss-of-function mutation using CRISPR-Cas9 technology to examine if the mice acquire skeletal segmentation anomalies and perform *in situ* hybridization of embryos to detect the transcription of *HOX* genes in the embryonic period. We aimed to explore the regulation between *FLNB* and *HOX* in the embryonic period, and to uncover the pathological mechanism of *FLNB*-related skeletal disorders.

2. Material and methods

2.1. Generation of mice model with *FLNB* G1586R mutation

The G1586R mutation in mouse *FLNB* (NM_001081427.1: c.4756G > A (p.Gly1586Arg)) is homologous to a pathogenic mutation site in human *FLNB* (NM_001457.3: c.4756G > A (p.Gly1586Arg)) that was previously reported by our group in a patient with severe skeletal malformation (Xu et al., 2018). The sgRNA target was designed around this point mutation site in exon 28 of mouse *FLNB* (Fig. 1a). The primers were synthesized according to the target sequence, and PCR was performed using the template of the gRNA framework to get the sequence of sgRNA. Then the transcription was performed *in vitro* using a T7 *in vitro* transcript kit (#E2050S, NEB, USA), and the sgRNA was purified after ethanol precipitation. The cleavage efficiency of sgRNA was tested using Cas9/gRNA *in-vitro* activity testing kit (#VK-007, ViewSolid, China), and the target sg1 (5'-tagctcgcggtcttatcaGGG-3') was screened with the

highest activity. The homologous recombination donor sequence was designed based on the sg1 target and point mutation sequence, and the donor ssDNA was synthesized. The transcripts of the sg1, Cas9 mRNA (#R001L, ViewSolid, China), and homologous recombined ssDNA were mixed, and the mixture was injected into the cytoplasm of the fertilized ovum. The fertilized ovum was transferred into the M2 culture solution to get diploid cells, and transplanted into the ovarian ducts of the recipient mice (ICR) to develop. The genomic DNA was isolated from the tail tips of 10-day-old mice. The point mutation in *FLNB* was genotyped using the following primers: 1F (5'-CATACAGAGGTGCCAAGTA-3') and 1R (5'-GACATTAAGTGGATAGAGAAGG-3') in F0 mice to get *FLNB*^{WT/G1586R} mice, which were then crossed to get heterozygous mice that can be passaged stably. All animal protocols followed the National Research Council's Guide for the Care and Use of Laboratory Animals, and was approved by the Animal Welfare and Ethics Committee of Peking Union Medical College Hospital (Ethics committee approval code: XHDW-2023-136).

2.2. Acquisition of bone marrow mononuclear cells and extraction of RNA and protein

FLNB^{WT/WT}, *FLNB*^{WT/G1586R}, and *FLNB*^{G1586R/G1586R} mice were euthanized. The femurs and tibias were collected, and the bone marrow was washed out. Red cells were lysed using ammonium chloride cell lysis buffer. The cell mixtures were filtered using 40 μm cell strainers to get the bone marrow cells. Total RNA was extracted with TRNzol universal total RNA extraction kit (cat No. DP424, TIANGEN, China). Total protein was extracted from bone marrow cells using RIPA buffer, and the protein concentration was determined with protein quantification kit (BCA).

2.3. Measurement of the transcription level of *FLNB* using Real-time PCR

cDNA was amplified from total RNA using PrimeScript™ RT Reagent Kit with gDNA Eraser (cat No. RR047A, Takara, Japan). The reverse-transcribed cDNA was amplified in a real-time fluorescence quantification PCR machine (Quantageneq225, Kubo, China) using Luna Universal

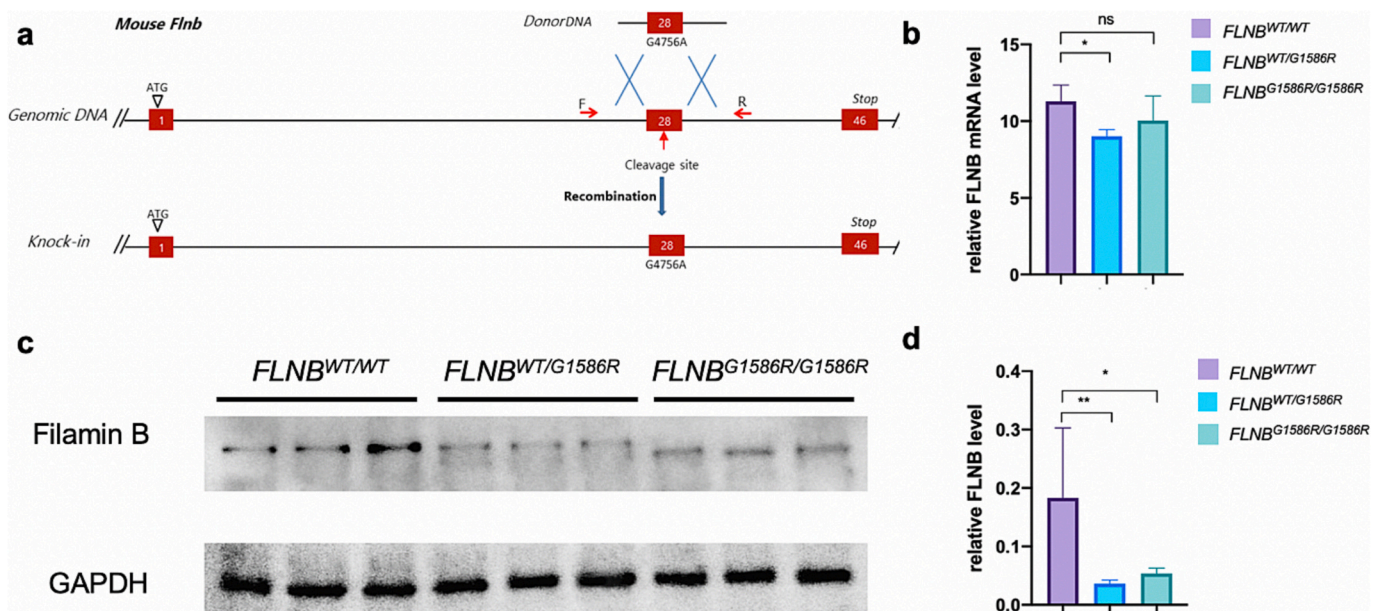


Fig. 1. Establishment of *FLNB*^{G1586R/G1586R} mice using CRISPR/Cas9. **a** Diagrammatic representation demonstrating that *FLNB* c.4756G>A was introduced into the genomic DNA using CRISPR/Cas9. **b** qPCR analysis of *FLNB* transcription in the bone marrow cells of *FLNB*^{WT/WT} mice, *FLNB*^{WT/G1586R} mice and *FLNB*^{G1586R/G1586R} mice (male, 33-week to 34-week, three mice for each group). **c-d** Western blot analysis of Filamin B and GAPDH expression in the bone marrow cells of *FLNB*^{WT/WT} mice, *FLNB*^{WT/G1586R} mice and *FLNB*^{G1586R/G1586R} mice (male, 33-week to 34-week, three mice for each group). The expression level of Filamin B was significantly down-regulated in the *FLNB*^{WT/G1586R} mice and *FLNB*^{G1586R/G1586R} mice, compared to *FLNB*^{WT/WT} mice.

qPCR Master Mix (cat No. M3003, NEB, USA). Primers used were as follows: *FLNB*: 5'-AGGACCCAGCAAGGTGGACATC-3' (sense) and 5'-CTTCCAGGCACATGCTCGTCAG-3' (antisense); *GAPDH*: 5'-ACACTGAGGACCAGTTGTCTCC-3' (sense) and 5'-TGTTGCTGTAGCCGTATTCATTGCA-3' (antisense). PCR conditions were as follows: 30 s at 95 °C, 45 cycles of 5 s at 95 °C, and 15 s at 60 °C. The amount of *FLNB* mRNA was normalized to *GAPDH* mRNA.

2.4. Measurement of the expression of *FLNB* using Western blotting

Western blotting was performed to measure the expression level of *FLNB*. The total protein was separated on an 8 % SDS-PAGE gel and transferred onto polyvinylidene difluoride (PVDF) membranes, which were then blocked and incubated with primary antibodies overnight. Primary antibodies used were anti-Filamin B (1:1000; cat No. ab224334, Abcam, UK), and anti-GAPDH (1:5000; cat No. 200306-7E4, Zen-Bio, China). The membranes were then incubated with HRP-conjugated goat anti-rabbit IgG (1:5000; cat No. 511203, Zen-Bio, China) or goat anti-mouse IgG (1: 5000; cat No. 511103, Zen-Bio, China) after a final wash, and developed in enhanced chemiluminescence reagent (Millipore).

2.5. Measurement of serum bone turnover markers

Mice were fasted for 6 h; blood was drawn, allowed to clot for 1 h, and centrifuged at 3000 rpm for 10 min. The serum levels of procollagen type 1 N-terminal propeptide (P1NP), osteocalcin (OCN), C-terminal telopeptides of type 1 collagen (CTX-1), and tartrate-resistant acid phosphatase 5b (TRACP5b) were measured using commercially available enzyme-linked immunosorbent assay (ELISA) kits (MEIMIAN, China) according to the instructions of the manufacturer.

2.6. Assessment of skeletal structure using micro-CT

For observation of skeletal structures, the distal left forelimbs and distal left hindlimbs were scanned by Inveon MM micro-CT manufactured by Siemens (Berlin, Germany) at a voltage of 70 kV and a current of 400 mA. Three-dimensional reconstruction was performed using the Inveon analysis workstation. For measurement of bone micro-architecture, the left hindlimbs were harvested from the mice above, and the midshaft and proximal metaphysis regions of the femur were scanned. The analysis was performed from 0.5 mm proximal to the growth plate, extending 1 mm towards the diaphysis. A spatial resolution of 35 μm was reconstructed using the Inveon analysis workstation. Trabecular volumetric bone mineral density (Tb.vBMD), cortical volumetric bone mineral density (Ct.vBMD), trabecular thickness (Tb.Th), trabecular separation (Tb.Sp), bone volume fraction (BV/TV), trabecular number (Tb.N), bone surface/volume (BS/BV), and cortical bone thickness (Ct.Th) were computed according to the instruction of the manufacturer. Three mice of each genotype were analyzed.

2.7. Histological observation

For histological observation on the carpal and tarsal bone, the distal right forelimbs and distal right hindlimbs were fixed in 4 % paraformaldehyde for 48 h at 4 °C, decalcified in 30 % methanoic acid for 24 h at 4 °C. Specimens were dehydrated and embedded in paraffin and sectioned at 4 μm, stained with hematoxylin and eosin, and observed using standard light microscope (Olympus, Japan). All images were captured through CaseViewer 2.4 software (3DHISTECH Ltd.). Three mice of each genotype were analyzed.

2.8. Whole skeletal preparation

Mice were dissected, skins were peeled away and all tissues were eviscerated. The remaining tissue was fixed in 95 % ethanol for 72 h, and

stained in 0.015 % alcian blue (Sigma-Aldrich, USA) dye for 96 h in dark at 37 °C. The carcasses were destained with 95 % ethanol for 8 h, and treated with 1 % KOH for 72 h until most soft tissue disappeared. After removing the remaining soft tissues with forceps, the mice were stained in 0.005 % alizarin red (Sigma-Aldrich, USA) solution for 96 h in dark. Finally, skeletons were cleared in a 20 % glycerol/1 % KOH solution for 12 h, and stored in 50 % ethanol/50 % glycerol for photography. Two mice of each genotype were analyzed.

2.9. *In situ* hybridization of embryos

Embryos (E12.5) of *FLNB*^{WT/WT}, *FLNB*^{WT/G1586R}, and *FLNB*^{G1586R/G1586R} mice were collected. Whole-mount *in situ* hybridization was performed as described (Wilkinson, 1992) with some modifications. Embryos were fixed with 4 % paraformaldehyde at 4 °C overnight. Embryos were then dehydrated and rehydrated through a methanol series. Further permeabilization was achieved by proteinase K treatment, followed by refixation. Digoxigenin-labeled (DIG-labeled) antisense riboprobes were generated from the mouse *HOXA4* gene (855-bp region amplified with 5'-CGGGATCCATGACCATGAGCTCGTTTTT-3' and 5'-CCCAAGCTTTATGGAGGAGGAATGGGTG-3'), *HOXB2* gene (1027-bp region amplified with 5'-CGGGATCCATGAATTTGAATTTGAGAG-3' and 5'-CCCAAGCTTTGAAGAAGTCCAGTCTTC-3'), *HOXB4* gene (750-bp region amplified with 5'-CGGGATCCATGGCTATGAGTTCCTTTTT-3' and 5'-CCCAAGCTTGAGCGCAGGGGGCCTCCGT-3'), *HOXD10* gene (1020-bp region amplified with 5'-CGGGATCCATGTCCTTTCCCAACAGCTC-3' and 5'-CCCAAGCTTAGAAAAGGTGAGTTGGC-3'). All 4 gene products above were cloned into the pSPT-18 vector (Roche), and DIG-labeled riboprobes were prepared as previously described (Wilkinson, 1992). Embryos were incubated with DIG-labeled probes in 70 °C humidified chamber overnight, with the unhybridized probes removed by washing, and the non-specific binding sites blocked with sheep serum. The bound probes were detected with an alkaline phosphatase substrate, antibody pre-absorption was omitted, and then incubated directly with the antibody overnight at 4 °C. Before development, embryos were washed with MABTL eight or more times for 1 h each at room temperature, then overnight at 4 °C to achieve lower backgrounds.

2.10. Statistical analysis

Continuous variables were expressed as mean ± standard deviations (SDs); Unpaired *t*-test was used for comparison between two groups. Two-tailed tests were used for all statistics, and *p* < 0.05 was defined as statistically significant differences. All figures were performed in GraphPad Prism 8.0 software (GraphPad, La Jolla, USA).

3. Results

3.1. Generation of mice with *FLNB* G1586R mutation

We have previously reported a patient with severe skeletal malformation including cervical kyphosis, scoliosis, and an increased number of carpal bones, with a missense mutation in *FLNB* (NM_001457.3, c.4756G > A (p.Gly1586Arg)) (Xu et al., 2018). To understand the role of *FLNB* in skeletal development, we generated *FLNB*^{G1586R/G1586R} mice using CRISPR/Cas9 (Fig. 1a). As shown in Fig. 1c and Fig. 1d, the protein level of Filamin B was significantly lowered in the *FLNB*^{WT/G1586R} mice and *FLNB*^{G1586R/G1586R} mice, compared to *FLNB*^{WT/WT} mice. We further performed q-PCR using the same samples. As shown in Fig. 1b, no significant difference in mRNA level was observed between *FLNB*^{G1586R/G1586R} mice and *FLNB*^{WT/WT} mice, indicating that the downregulation of *FLNB* was not a result of reduced transcription of a mutant gene, but was more likely caused by reduced mRNA translation or increased protein degradation.

3.2. Short stature in $FLNB^{G1586R/G1586R}$ mice

We measured the body weights and body lengths of 3 $FLNB^{WT/WT}$, 3 $FLNB^{WT/G1586R}$, and 2 $FLNB^{G1586R/G1586R}$ male mice every week from ages 7 weeks to 37 weeks. As shown in Fig. 2, the body weights of $FLNB^{G1586R/G1586R}$ mice were lower than $FLNB^{WT/G1586R}$ mice and $FLNB^{WT/WT}$ mice, and the body lengths of $FLNB^{G1586R/G1586R}$ mice were shorter than $FLNB^{WT/G1586R}$ mice and $FLNB^{WT/WT}$ mice. These findings suggested that $FLNB^{G1586R/G1586R}$ led to the short stature of mice during development.

3.3. Skeletal malformations in $FLNB^{G1586R/G1586R}$ mice

We performed micro-CT, HE staining and whole skeletal preparation in $FLNB^{WT/WT}$, $FLNB^{WT/G1586R}$, and $FLNB^{G1586R/G1586R}$ mice. As shown in Fig. 3, tarsal bones were separated in $FLNB^{WT/WT}$ mice; while those tarsal bones were fused in $FLNB^{WT/G1586R}$ mice and $FLNB^{G1586R/G1586R}$ mice. As shown in Figs. S1 and S2, the morphology of carpal bones and vertebrae were not significantly different among $FLNB^{WT/WT}$ mice, $FLNB^{WT/G1586R}$ mice and $FLNB^{G1586R/G1586R}$ mice. These results indicated that $FLNB^{G1586R/G1586R}$ led to the fusion of tarsal bones during development.

We measured the bone microarchitecture parameters in $FLNB^{WT/WT}$ mice, $FLNB^{WT/G1586R}$ mice and $FLNB^{G1586R/G1586R}$ mice. The trabecular volumetric BMD (Tb.vBMD) was significantly lower in $FLNB^{G1586R/G1586R}$ mice compared to $FLNB^{WT/WT}$ mice. The trabecular thickness (Tb.Th) in the $FLNB^{G1586R/G1586R}$ mice had a trend of downregulation, and

the trabecular separation (Tb.Sp) in the $FLNB^{G1586R/G1586R}$ mice had a trend of upregulation, compared to $FLNB^{WT/WT}$ mice, though not statistically significant (Fig. 4). This indicated that the bone microarchitecture had deteriorated in $FLNB^{G1586R/G1586R}$ mice.

We also measured the serum bone turnover markers in $FLNB^{WT/WT}$ mice, $FLNB^{WT/G1586R}$ mice and $FLNB^{G1586R/G1586R}$ mice (Fig. S3). Serum bone formation indexes, P1NP and OCN, presented a trend of downregulation in the $FLNB^{G1586R/G1586R}$ mice compared to $FLNB^{WT/WT}$ mice; and bone resorption indexes, CTX-1 and TRACP5b, presented a trend of upregulation in the $FLNB^{G1586R/G1586R}$ mice compared to $FLNB^{WT/WT}$ mice, though the differences were not statistically significant.

3.4. *In situ* hybridization of HOX genes in embryos

HOXD10 is a key gene regulating the segmentation of the forelimb and hindlimb (Quinonez and Innis, 2014; Wellik and Capecchi, 2003). We performed *in situ* hybridization of embryos (E12.5) of *HOXD10* in $FLNB^{WT/WT}$, $FLNB^{WT/G1586R}$, and $FLNB^{G1586R/G1586R}$ mice (Fig. 5). In the metacarpal bones and carpal bones of the forelimb in E12.5, the staining area of *HOXD10* was smaller and the staining was weaker in $FLNB^{G1586R/G1586R}$ mice compared with $FLNB^{WT/WT}$ mice and $FLNB^{WT/G1586R}$ mice. This indicated that the transcription level of *HOXD10* was downregulated in $FLNB^{G1586R/G1586R}$ mice during the embryonic development of carpal bone.

HOXB2, *HOXA4*, and *HOXB4* are key genes in the development of cervical spine (Quinonez and Innis, 2014). We performed *in situ* hybridization of embryos (E12.5) of *HOXB2*, *HOXA4*, and *HOXB4* in

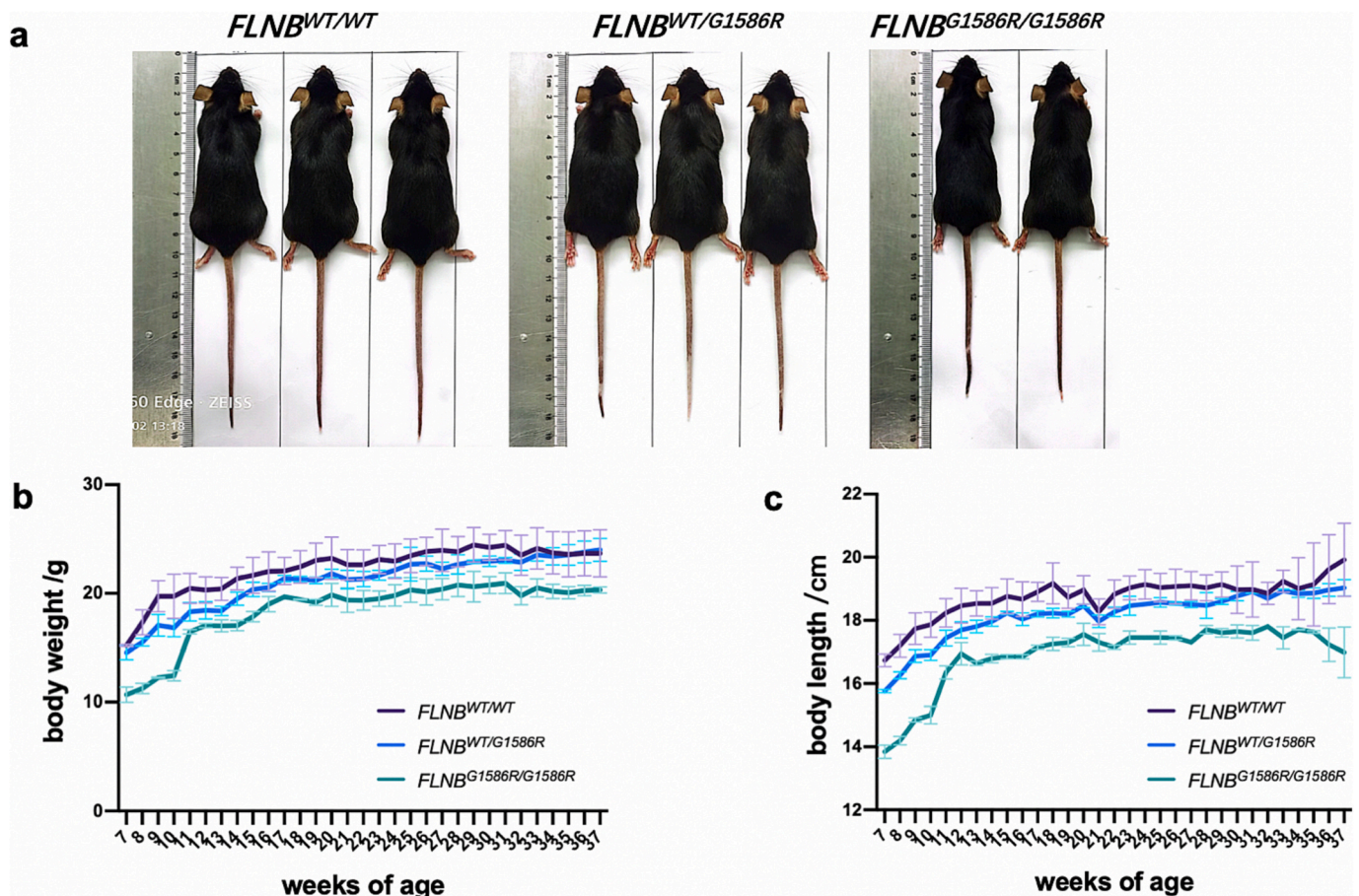


Fig. 2. Body weight and body length of the $FLNB^{WT/WT}$ mice, $FLNB^{WT/G1586R}$ mice and $FLNB^{G1586R/G1586R}$ mice. a Gross pictures of 3 $FLNB^{WT/WT}$, 3 $FLNB^{WT/G1586R}$ and 2 $FLNB^{G1586R/G1586R}$ mice (male, 37-week). b-c Graphical representation of the body weights and body lengths of 3 $FLNB^{WT/WT}$, 3 $FLNB^{WT/G1586R}$ and 2 $FLNB^{G1586R/G1586R}$ mice (male, from 7-week to 37-week). The body weights of $FLNB^{G1586R/G1586R}$ mice were lower than $FLNB^{WT/G1586R}$ mice and $FLNB^{WT/WT}$ mice, and the body lengths of $FLNB^{G1586R/G1586R}$ mice were shorter than $FLNB^{WT/G1586R}$ mice, and $FLNB^{WT/WT}$ mice.

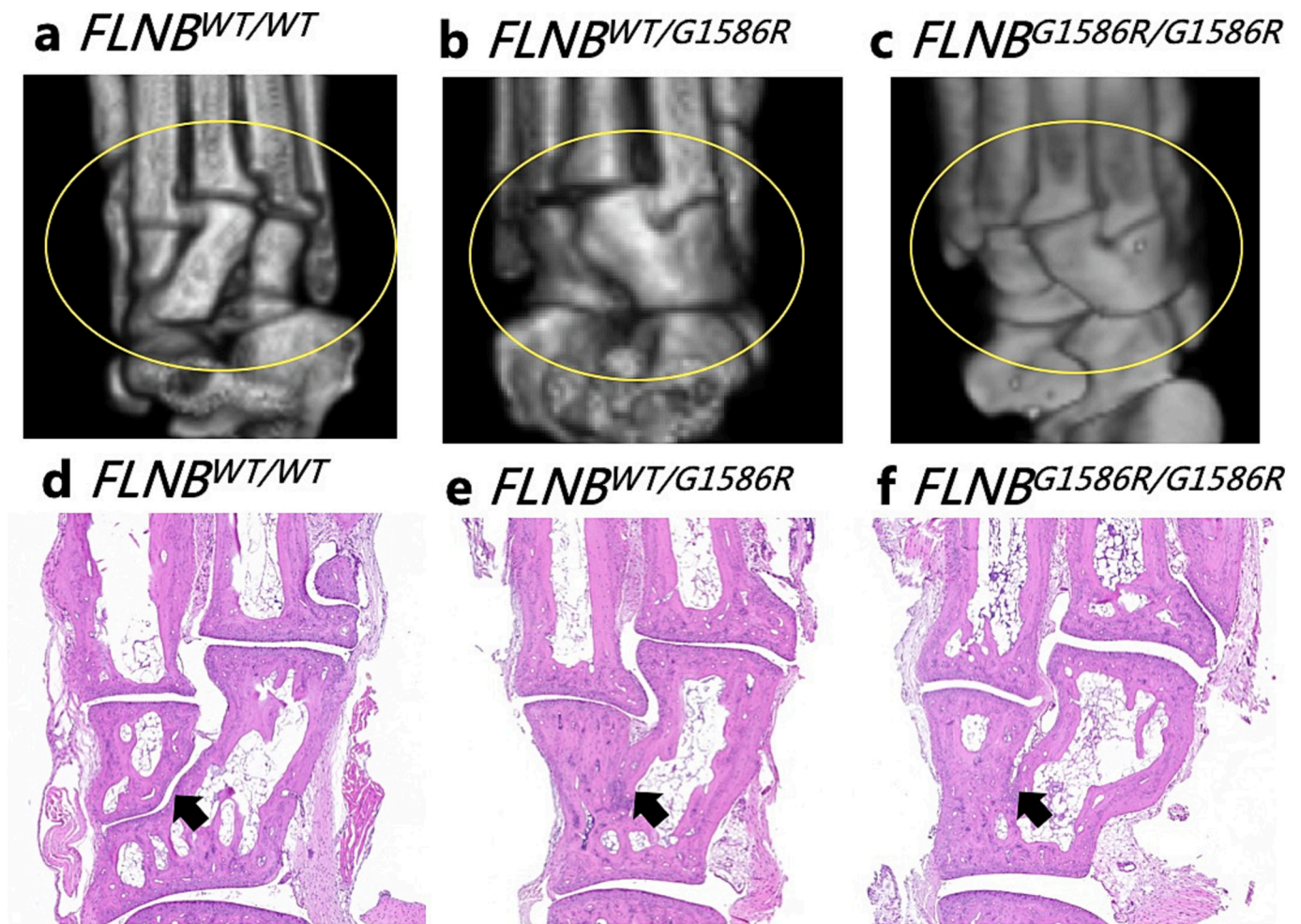


Fig. 3. Micro-CT three dimensional reconstruction of tarsal bones, and hematoxylin and eosin (HE) staining of tarsal bones of the $FLNB^{WT/WT}$ mice, $FLNB^{WT/G1586R}$ mice and $FLNB^{G1586R/G1586R}$ mice (3 male mice in each group, 8-week). In the plantar view of hindlimb, tarsal bones (indicated in oval) were separated in the $FLNB^{WT/WT}$ mice (a, d); while tarsal bones (indicated in oval) were fused in $FLNB^{WT/G1586R}$ mice (b, e) and $FLNB^{G1586R/G1586R}$ mice (c, f);

$FLNB^{WT/WT}$ mice, $FLNB^{WT/G1586R}$ mice, and $FLNB^{G1586R/G1586R}$ mice (Fig. S4). In the cervical spine, the staining area of *HOXB2* was smaller in $FLNB^{G1586R/G1586R}$ mice compared with $FLNB^{WT/WT}$ mice and $FLNB^{WT/G1586R}$, while the staining of *HOXA4* and *HOXB4* was not significantly different in $FLNB^{G1586R/G1586R}$ mice compared with $FLNB^{WT/WT}$ mice and $FLNB^{WT/G1586R}$. These findings indicated that *HOXB2* was down-regulated in $FLNB^{G1586R/G1586R}$ mice during the embryonic development of the cervical spine.

4. Discussion

4.1. Summary of the study

In this study, we established a mouse model with a loss-of-function mutation in *FLNB* using CRISPR/Cas9 technology. The mouse model presented short stature and fusions in tarsal bones, which phenocopied human disease SCT syndrome. We further found that the transcription of different *HOX* gene subtypes was downregulated in the embryo of mice with loss-of-function *FLNB*, using *in situ* hybridization of embryos. The findings above indicated that disruption of *FLNB* may lead to disorders in skeletal segmentation by regulating the expression of *HOX* genes.

4.2. Comparison to previous *FLNB*-deficient mice models

Previous researchers have generated *FLNB*-knockout mice models

before (Farrington-Rock et al., 2008; Zhou et al., 2007). The model by Farrington-Rock et al. presented fusions in carpal bones and vertebrae, and the model by Zhou et al. presented fusions in vertebrae but no fusions in carpal and tarsal (though reductions in hyaline cartilage in ribs, metacarpals, phalanges, and tarsals were found). In our mouse model, instead of using a gene-trap vector to knock out the *FLNB* gene, we used CRISPR/Cas9 technology to introduce a known pathogenic point mutation G1586R into *FLNB* and down-regulated the expression of *FLNB*. We observed fusions in tarsal bones, which was similar to previous findings in *FLNB*-deficient mice models, but we did not find obvious fusions in vertebrae in the model. The possible reason may be that in previous models the actin-binding domain (ABD) of *FLNB* was dysfunctional, while in our model the point mutation G1586R was located in repeat-14 of *FLNB*, which did not lead to a complete loss-of-function in *FLNB*, so that the skeletal segmentation was not significantly interfered.

4.3. Known mechanisms of *FLNB* in causing skeletal malformation

There have been several mechanisms proposed by previous researchers explaining how *FLNB* regulated skeletal development. ① *Loss-of-function mutation in FLNB leads to abnormal growth in the growth plate of long bone.* Hu et al. found that in the mouse model with loss-of-function in *FLNB*, the proliferation zone of the growth plate of the long bone became narrow, while the differentiated hypertrophic zone became

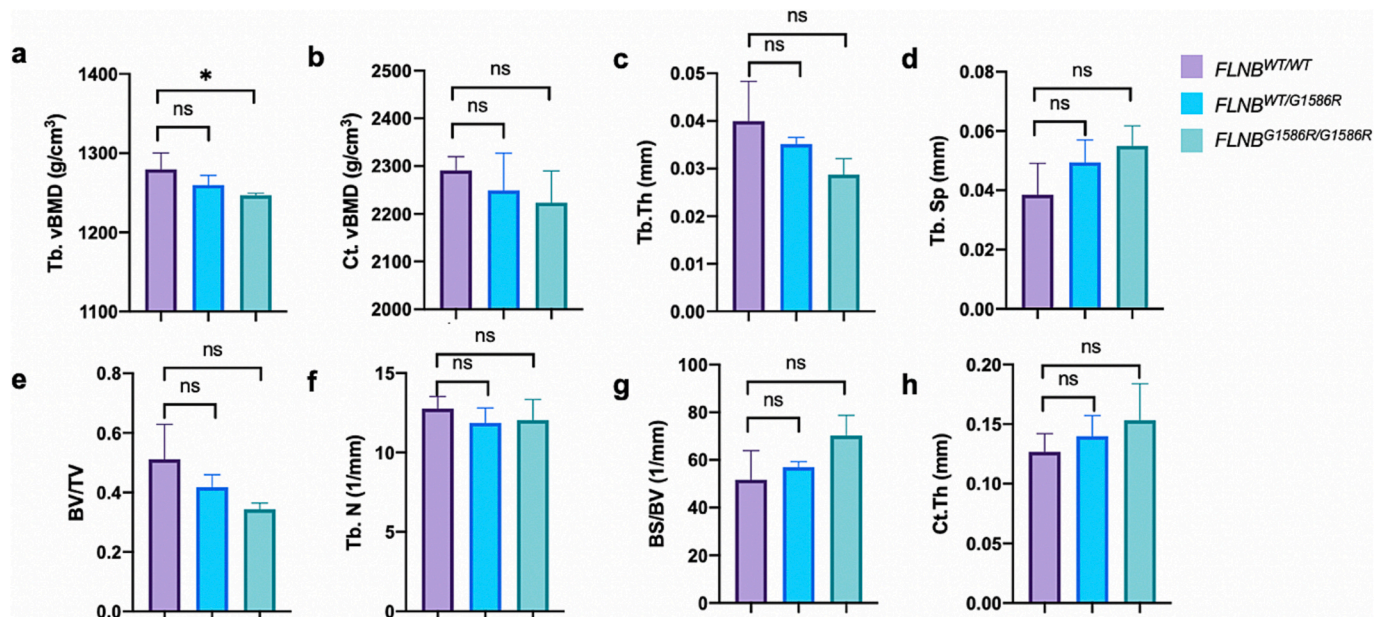


Fig. 4. Bone microarchitecture parameters in *FLNB*^{WT/WT} mice, *FLNB*^{WT/G1586R} mice and *FLNB*^{G1586R/G1586R} mice (3 male mice in each group, 8-week). Tb.vBMD was significantly lower in *FLNB*^{G1586R/G1586R} mice compared to *FLNB*^{WT/WT} mice. Tb.Th in the *FLNB*^{G1586R/G1586R} mice had a trend of downregulation, and Tb.Sp in the *FLNB*^{G1586R/G1586R} mice had a trend of upregulation, compared to *FLNB*^{WT/WT} mice, though not statistically significant. Abbreviations: Trabecular volumetric bone mineral density (Tb.vBMD), cortical volumetric bone mineral density (Ct.vBMD), trabecular thickness (Tb.Th), trabecular separation (Tb.Sp), bone volume fraction (BV/TV), trabecular number (Tb.N), bone surface/volume (BS/BV), and cortical bone thickness (Ct.Th).

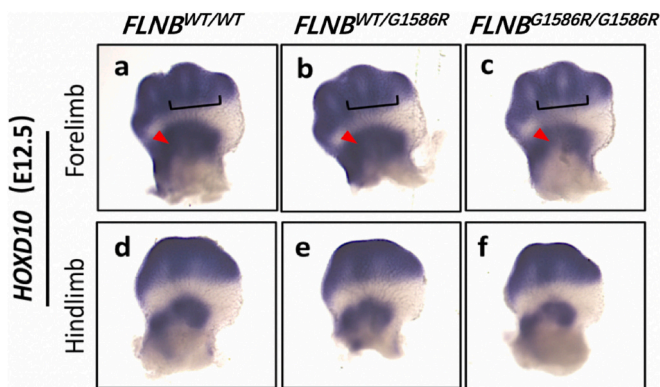


Fig. 5. *In situ* hybridization of embryo (E12.5) of *HOXD10* in *FLNB*^{WT/WT} mice, *FLNB*^{WT/G1586R} mice and *FLNB*^{G1586R/G1586R} mice. (a-c) In the metacarpal bones (pointed by black bracket) and carpal bones (pointed by red arrow) of forelimb, the staining area of *HOXD10* was smaller and the staining of *HOXD10* was weaker in *FLNB*^{G1586R/G1586R} mice compared with *FLNB*^{WT/WT} mice and *FLNB*^{WT/G1586R}. (d-f) In the metatarsal bones and tarsal bones of hindlimb, the staining of *HOXD10* was not significantly different in *FLNB*^{G1586R/G1586R} mice compared with *FLNB*^{WT/WT} mice and *FLNB*^{WT/G1586R}.

broadened, and the osteogenic capacity was reduced (Hu et al., 2014). In addition, Lu et al. found that the apoptosis rate of chondrocytes was significantly increased in the hypertrophic zone of the radius of the mice with loss-of-function in *FLNB* (Lu et al., 2007). These findings explained why the length and diameter of the long bone are smaller in patients with SCT syndrome. © Gain-of-function mutation in *FLNB* leads to the enhancement of binding of *FLNB* and actin and affects the migration of cell skeleton. Daniel et al. and Sawyer et al. found the missense mutation in the binding domain of *FLNB* with actin leads to increased binding capacity with actin, which was associated with skeletal malformation (Daniel et al., 2012; Sawyer et al., 2009). Those studies above, though interesting, only explained the phenotype of short stature in *FLNB*-deficient patients, but did not explain why the number of ossification

centers was abnormal (i.e. why the skeletal segmentation was abnormal) in *FLNB*-related skeletal disorders.

4.4. *HOX* genes and skeletal malformation

The skeletal segmentation in the embryonic period of vertebral animals is known to be regulated by *HOX* genes (Quinonez and Innis, 2014). Different *HOX* genes express in different stages and different segments in the embryonic period and regulate segmentation of the skeleton and other tissues. For example, loss of function in Group 4 to 9 paralogues of *HOX* genes leads to malformations in cervical, thoracic, and lumbar vertebrae; loss of function in *HOXD11* leads to fusion in carpal and fusion in the distal radius and ulna; and loss of function in *HOXD12* and *HOXD13* leads to fusion in the carpal and metacarpal and shortening of phalanges. Interestingly, the skeletal malformation phenotypes were remarkably similar between the *HOX*-mutated spectrum disorders and *FLNB*-mutated spectrum disorders, both of which were characterized by alterations in the number of ossification centers. Therefore, we studied whether loss of function in *FLNB* interfered with transcription of *HOX* in the embryonic period.

4.5. Loss of function in *FLNB* interferes with transcription of the *HOX* gene

In this study, we found that the transcription level of *HOXD10* was downregulated in the metacarpal bones and carpal bones of the *FLNB*^{G1586R/G1586R} mice during the embryonic development of carpal bone, and the transcription of *HOXB2* was downregulated in *FLNB*^{G1586R/G1586R} mice during the embryonic development of cervical spine (Figs. 5, S4). *HOXD10* is a key gene regulating the segmentation of the forelimb and hindlimb, and *HOXB2* is a key gene regulating the segmentation of the cervical spine (Quinonez and Innis, 2014; Wellik and Capecchi, 2003). Those findings above suggested that loss of function in *FLNB* may lead to disorders in the segmentation through *HOX* genes during the embryonic period, which first established a link between *FLNB* and *HOX* gene.

In the metatarsal bones and tarsal bones of the hindlimb, the

transcription level of *HOXD10* was not significantly different in *FLNB*^{G1586R/G1586R} mice compared with *FLNB*^{WT/WT} mice and *FLNB*^{WT/G1586R} (Fig. 5). The development of the hindlimb is usually earlier than the forelimb by around half a day, so we assume the segmentation of the hindlimb has been finished by E12.5, so the expression of *HOXD10* was not different in *FLNB*^{G1586R/G1586R} mice compared to *FLNB*^{WT/WT} mice and *FLNB*^{WT/G1586R}.

4.6. How does *FLNB* regulate *HOX* in skeletal development?

Until now, no studies have reported the direct interaction between *FLNB* and *HOX*. However, there were some clues indicating that connections between *FLNB* and *HOX* might exist through the BMP-Smad signaling pathway. Zheng et al. have reported that *FLNB* regulated the phosphorylation of Smad. When loss of function occurred in *FLNB*, the free phosphorylated Smad was increased in the cytoplasm, which increased the transcription activity of Runx2 (Zheng et al., 2007). In addition, Li et al. have reported that *HOX* proteins were downstream DNA-binding proteins in the BMP signaling cascade and the transcriptional activities of *HOX* were regulated by Smads (Li et al., 2006). Therefore, we hypothesize that loss of function in *FLNB* may up-regulate the phosphorylation of Smad, down-regulate the transcription function of *HOX* gene, and therefore inhibit the skeletal segmentation in the embryonic period and lead to skeletal malformation.

There were also other studies indicating that *FLNB* may regulate *HOX* through actin. It is known that *FLNB*, a scaffold protein, assists in the rearrangement of F-actin in the cytoplasm (Zhao et al., 2016). Ferrai et al. have reported that inhibition of actin polymerization blocked the transcription of *HOXB* genes (Ferrai et al., 2009). And Miyamoto et al. has found that knock-down of an actin-binding protein resulted in defective *HOX* gene action and abnormal embryonic development (Miyamoto et al., 2013). Therefore, we hypothesize that loss of function in *FLNB* may interfere with the polymerization of actin, down-regulate the transcription of *HOX* gene, and lead to abnormal embryonic skeletal segmentation. However, further experiments need to be performed to test if *FLNB* truly regulates the activity of *HOX* gene through either the BMP-Smad signaling cascade or through actin polymerization.

4.7. Strengths and limitations

There were several strengths in the study. We first established a mouse model with a pathogenic point mutation G1586R in *FLNB* using CRISPR/Cas9 technology, which presented loss of function in *FLNB* and skeletal malformations including short stature and fusions in tarsal bones. We first established a link between *FLNB* and *HOX*, showing that *FLNB* may regulate skeletal segmentation through *HOX* gene. Besides, the point mutation G1586R we introduced to *FLNB* was located in the repeat-14 of *FLNB*. Previous studies always focused on the mutations in the actin-binding domain (ABD) of *FLNB*, but our study indicated that functions in other domains in *FLNB* were also important and worth further exploration.

There were also limitations in the study. The sample size of experiments in this study was relatively small. This was due to the low survival rate of mice with a homozygous mutation in *FLNB*, and further experiments should be performed at different stages of the life cycle of the mice with a larger sample size. Besides, since *HOXD10* is a key gene regulating the segmentation of the forelimb and hindlimb, we mainly focused on the transcription level of *HOXD10* gene in the embryonic development of carpal bones and tarsal bones, but didn't test other *HOX* gene subtypes which were also responsible for this segmentation process. In addition, we did not further explain how *FLNB* exactly regulates *HOX* gene, which needed further experiments to study.

In conclusion, we generated a mouse model with a loss-of-function mutation in *FLNB*, which showed a shorter stature, and fusions in tarsal bones, and partially phenocopied *FLNB*-related skeletal disorders in humans. The transcription of *HOXD10* was downregulated in the

regions of the metacarpal and carpal regions during embryonic development. Loss of function in *FLNB* may lead to skeletal malformation by interfering with skeletal segmentation through *HOX* genes.

Declaration of generative AI in scientific writing

We declare that no AI or AI-assisted technologies were used in the writing process of the manuscript.

CRediT authorship contribution statement

Qiming Xu: Writing – review & editing, Supervision, Project administration, Conceptualization. **Lijia Cui:** Writing – original draft, Funding acquisition, Formal analysis, Data curation. **Yude Lin:** Data curation. **Leigh-Anne Cui:** Data curation. **Weibo Xia:** Writing – review & editing, Supervision, Funding acquisition, Conceptualization.

Declaration of competing interest

Lijia Cui, Yude Lin, Leigh-Anne Cui, Weibo Xia, Qiming Xu declare no conflict of interest.

Data availability

All data are available from the corresponding authors upon reasonable request.

Acknowledgement

We acknowledge Dr. Yujie Shi from the Scripps Research Institute for her important instruction in the experimental design. This research was supported by the National Natural Science Foundation of China (LC, 82100946; WX, 82270938), Bethune Charitable Foundation (LC, G-X-2020-1107-16), Young Elite Scientists Sponsorship Program by BAST (LC, No.BYESS2023171), CAMS Innovation Fund for Medical Sciences (WX, 2021-I2M-1-002), National Key Research and Development Program of China (WX, 2021YFC2501700), National High Level Hospital Clinical Research Funding (WX, 2022-PUMCH-D-006), and the Non-profit Central Research Institute Fund of the Chinese Academy of Medical Sciences (LC, 2023-PT320-10).

Appendix A. Supplementary data

Supplementary data to this article can be found online at <https://doi.org/10.1016/j.bonr.2024.101746>.

References

- Daniel, P.B., Morgan, T., Alanay, Y., Bijlsma, E., Cho, T.J., Cole, T., Collins, F., David, A., Devriendt, K., Faivre, L., Ikegawa, S., Jacquemont, S., Jelic, M., Krakow, D., Liebrecht, D., Maitz, S., Marlin, S., Morin, G., Nishikubo, T., Nishimura, G., Prescott, T., Scarano, G., Shafeghati, Y., Skovby, F., Tsutsumi, S., Whiteford, M., Zenker, M., Robertson, S.P., 2012. Disease-associated mutations in the actin-binding domain of filamin B cause cytoplasmic focal accumulations correlating with disease severity. *Hum. Mutat.* 33 (4), 665–673.
- Farrington-Rock, C., Kirilova, V., Dillard-Telm, L., Borowsky, A.D., Chalk, S., Rock, M.J., Cohn, D.H., Krakow, D., 2008. Disruption of the *Flnb* gene in mice phenocopies the human disease spondylocarpotarsal synostosis syndrome. *Hum. Mol. Genet.* 17 (5), 631–641.
- Ferrai, C., Naum-Onganía, G., Longobardi, E., Palazzolo, M., Disanza, A., Diaz, V.M., Crippa, M.P., Scita, G., Blasi, F., 2009. Induction of *HoxB* transcription by retinoic acid requires actin polymerization. *Mol. Biol. Cell* 20 (15), 3543–3551.
- Hu, J., Lu, J., Lian, G., Ferland, R.J., Dettenhofer, M., Sheen, V.L., 2014. Formin 1 and filamin B physically interact to coordinate chondrocyte proliferation and differentiation in the growth plate. *Hum. Mol. Genet.* 23 (17), 4663–4673.
- Jeon, G.W., Lee, M.N., Jung, J.M., Hong, S.Y., Kim, Y.N., Sin, J.B., Ki, C.S., 2014. Identification of a de novo heterozygous missense *FLNB* mutation in lethal atelosteogenesis type 1 by exome sequencing. *Ann. Lab. Med.* 34 (2), 134–138.
- Kozłowski, K., Tsuruta, T., Kameda, Y., Kan, A., Leslie, G., 1981. New forms of neonatal death dwarfism. Report of 3 cases. *Pediatr. Radiol.* 10 (3), 155–160.

- Kozlowski, K., Silience, D., Cortis-Jones, R., Osborn, R., 1985. Boomerang dysplasia. *Br. J. Radiol.* 58 (688), 369–371.
- Krakow, D., Robertson, S.P., King, L.M., Morgan, T., Sebald, E.T., Bertolotto, C., Wachsmann-Hogiu, S., Acuna, D., Shapiro, S.S., Takafuta, T., Aftimos, S., Kim, C.A., Firth, H., Steiner, C.E., Cormier-Daire, V., Superti-Furga, A., Bonafe, L., Graham Jr., J.M., Grix, A., Bacino, C.A., Allanson, J., Bialer, M.G., Lachman, R.S., Rimoin, D.L., Cohn, D.H., 2004. Mutations in the gene encoding filamin B disrupt vertebral segmentation, joint formation and skeletogenesis. *Nat. Genet.* 36 (4), 405–410.
- Larsen, L.J., Schottstaedt, E.R., Bost, F.C., 1950. Multiple congenital dislocations associated with characteristic facial abnormality. *J. Pediatr.* 37 (4), 574–581.
- Li, X., Nie, S., Chang, C., Qiu, T., Cao, X., 2006. Smads oppose Hox transcriptional activities. *Exp. Cell Res.* 312 (6), 854–864.
- Lu, J., Lian, G., Lenkinski, R., De Grand, A., Vaid, R.R., Bryce, T., Stasenko, M., Boskey, A., Walsh, C., Sheen, V., 2007. Filamin B mutations cause chondrocyte defects in skeletal development. *Hum. Mol. Genet.* 16 (14), 1661–1675.
- Maroteaux, P., Spranger, J., Stanesco, V., Le Marec, B., Pfeiffer, R.A., Beighton, P., Mattei, J.F., 1982. Atelosteogenesis. *Am. J. Med. Genet.* 13 (1), 15–25.
- Miyamoto, K., Teperek, M., Yusa, K., Allen, G.E., Bradshaw, C.R., Gurdon, J.B., 2013. Nuclear Wave1 is required for reprogramming transcription in oocytes and for normal development. *Science* 341 (6149), 1002–1005.
- Quinonez, S.C., Innis, J.W., 2014. Human HOX gene disorders. *Mol. Genet. Metab.* 111 (1), 4–15.
- Sawyer, G.M., Clark, A.R., Robertson, S.P., Sutherland-Smith, A.J., 2009. Disease-associated substitutions in the filamin B actin binding domain confer enhanced actin binding affinity in the absence of major structural disturbance: insights from the crystal structures of filamin B actin binding domains. *J. Mol. Biol.* 390 (5), 1030–1047.
- Stanley, C.S., Thelin, J.W., Miles, J.H., 1988. Mixed hearing loss in Larsen syndrome. *Clin. Genet.* 33 (5), 395–398.
- Stosel, T.P., Condeelis, J., Cooley, L., Hartwig, J.H., Noegel, A., Schleicher, M., Shapiro, S.S., 2001. Filamins as integrators of cell mechanics and signalling. *Nat. Rev. Mol. Cell Biol.* 2 (2), 138–145.
- Tenconi, R., Kozlowski, K., Largaiolli, G., 1983. Boomerang dysplasia. A new form of neonatal death dwarfism. *Rof. 138* (3), 378–380.
- Wellik, D.M., Capecchi, M.R., 2003. Hox10 and Hox11 genes are required to globally pattern the mammalian skeleton. *Science* 301 (5631), 363–367.
- Wilkinson, D.G., 1992. Whole mount in situ hybridization of vertebrate embryos. In: Wilkinson, D.G. (Ed.), *In Situ Hybridization: A Practical Approach*. Oxford University Press, New York, pp. 89–99.
- Xu, Q., Wu, N., Cui, L., Wu, Z., Qiu, G., 2017. Filamin B: the next hotspot in skeletal research? *J. Genet. Genomics* 44 (7), 335–342.
- Xu, Q., Wu, N., Cui, L., Lin, M., Thirumal Kumar, D., Doss, C., George Priya, Wu, Z., Shen, J., Song, X., Qiu, G., 2018. Comparative analysis of the two extremes of FLNB-mutated autosomal dominant disease spectrum: from clinical phenotypes to cellular and molecular findings. *Am. J. Transl. Res.* 10 (5), 1400–1412.
- Zhao, Y., Shapiro, S.S., Eto, M., 2016. F-actin clustering and cell dysmotility induced by the pathological W148R missense mutation of filamin B at the actin-binding domain. *Am. J. Phys. Cell Phys.* 310 (1), C89–C98.
- Zheng, L., Baek, H.J., Karsenty, G., Justice, M.J., 2007. Filamin B represses chondrocyte hypertrophy in a Runx2/Smad3-dependent manner. *J. Cell Biol.* 178 (1), 121–128.
- Zhou, X., Tian, F., Sandzen, J., Cao, R., Flaberg, E., Szekely, L., Cao, Y., Ohlsson, C., Bergo, M.O., Boren, J., Akyurek, L.M., 2007. Filamin B deficiency in mice results in skeletal malformations and impaired microvascular development. *Proc. Natl. Acad. Sci. USA* 104 (10), 3919–3924.